



## Atmospheric Effects of the Kuroshio Large Meander during 2004–05\*

HAIMING XU

*Key Laboratory of Meteorological Disaster and College of Atmospheric Sciences, Nanjing University of Information Science and Technology, Nanjing, China*

HIROKI TOKINAGA

*International Pacific Research Center, University of Hawaii at Manoa, Honolulu, Hawaii*

SHANG-PING XIE

*International Pacific Research Center, and Department of Meteorology, University of Hawaii at Manoa, Honolulu, Hawaii*

(Manuscript received 29 May 2009, in final form 15 April 2010)

### ABSTRACT

In the summer of 2004, the Kuroshio took a large meander path south of Japan for the first time since 1991, and this large meander event persisted until the next summer. Satellite observations and numerical model simulations are used to study the effect of this large meander event on the atmosphere. The large meander leaves a cool water pool between the Kuroshio and Japanese coast. Sea surface temperature (SST) in the cool water pool is about 2°–3°C colder than the surroundings during winter and spring, whereas the SST signature substantially weakens in summer. A local reduction of wind speed is found over the cool water pool, and the positive SST–wind speed correlation is indicative of ocean forcing of the atmosphere. Cloud liquid water (CLW) content and precipitation also decrease over the cool SST pool.

A regional atmospheric model successfully simulates atmospheric response to the Kuroshio large meander. The model experiments suggest that the reduced surface wind speed and precipitation are due to the large meander-induced SST cooling. Analysis of the surface perturbation momentum budgets shows the importance of the pressure adjustment mechanism in surface wind response to the cold SST anomalies.

### 1. Introduction

The Kuroshio Extension, the western boundary current of the North Pacific subtropical gyre, flows north-eastward along the continental slope of the East China Sea, turns east through Tokara Strait, and proceeds eastward along the southern coast of Japan until it separates from the coast and enters the Pacific basin. It is well known that the Kuroshio south of Japan exhibits

remarkable bimodal behavior between the large meander (LM) and the nonlarge meander (NLM) paths (Taft 1972; Kawabe 1985). The LM path displaces offshore south of Japan, whereas the NLM path hugs the coast of Kyushu and Shikoku until leaving the coast at Cape Shiono-misaki. Once formed, both the LM and NLM paths can persist over a period ranging from a few years to a decade. In contrast, the transition between the two paths is rapid, often taking place over a period of several months (Kawabe 1986).

The Kuroshio path bimodality is due to complicated interactions of the current, its potential vorticity advection, bathymetry, and coastline inclination (Chao 1984; Kawabe 1996). Some studies suggest that the Kuroshio takes the LM (NLM) path when the upstream inflow transport is large (small) (Yamagata and Umatani 1989; Sekine 1990; Akitomo et al. 1991; Kawabe 1996). While Kuroshio bimodality studies so far have exclusively been

---

\* International Pacific Research Center Publication Number 695 and School of Ocean and Earth Science and Technology Publication Number 7934.

---

*Corresponding author address:* Dr. Haiming Xu, College of Atmospheric Sciences, Nanjing University of Information Science and Technology, 219 Ning Liu Road, Nanjing 210044, China.  
E-mail: haimingx@gmail.com

oceanographic in nature, the path change, resulting in a sea surface temperature (SST) change of a few degrees Celsius, is likely to cause a significant atmospheric response. Such atmospheric effects, however, have never been documented in the literature, largely because of the lack of comprehensive observations.

In the summer (June–August) of 2004, a large meander with 800–1000-km length took place for the first time since 1991 and persisted until the next summer. A small meander southeast of Kyushu that occurred in December 2003 triggered the subsequent development of a large meander (Usui et al. 2008). This large meander event is the first and only event observed by a suite of satellite-borne microwave sensors including altimeters, the Tropical Rain Measuring Mission (TRMM) Microwave Imager (TMI), and the Quick Scatterometer (QuickSCAT). These microwave sensors see through clouds and offer a view of ocean–atmosphere interactions in unprecedented detail (Wentz et al. 2000; Nonaka and Xie 2003; Chelton et al. 2004; Xie 2004).

The present note examines atmospheric influences of the Kuroshio LM event of 2004–05, taking advantage of these satellite observations. We show that the LM produces large anomalies in SST, surface wind, cloud, and precipitation. We use a regional atmospheric model, which successfully simulates the observed atmospheric response, to investigate the LM effect on the atmosphere. In the rest of the note, section 2 describes the satellite data, section 3 presents results of the satellite data analysis, section 4 describes an atmospheric model and presents its simulations, and section 5 is a summary.

## 2. Data

This study uses satellite observations of SST, sea surface height (SSH), sea surface wind, cloud liquid water (CLW), and precipitation by microwave sensors on different platforms. The TMI measures SST free of clouds over the global tropics within 38°N/S. It also measures rain rate and column-integrated cloud liquid water content. We use a monthly TMI product on a 0.25° grid (Wentz et al. 2000). The microwave scatterometer on the QuikSCAT satellite measures daily surface wind velocity over the World Ocean (Liu et al. 2000). We use a monthly product of wind velocity on a 0.25° grid from a remote sensing system. Altimeters on the European Remote Sensing (ERS), Ocean Topography Experiment (TOPEX)/Poseidon (T/P), and JASON satellites measure SSH deviations from their long-term mean at nadir. We use a SSH dataset merging all available altimeter observations (Ducet et al. 2000) from January 1992 on a 0.25° grid. A mean SSH product

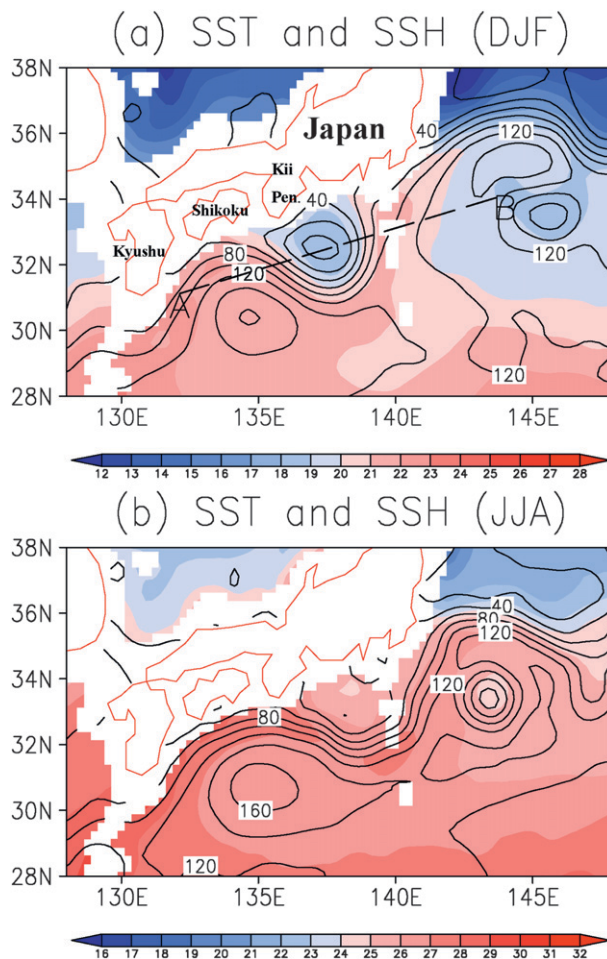


FIG. 1. Seasonal mean TMI sea surface temperature (shaded, °C) and sea surface height (contours at 20-cm intervals) in (a) the winter (December–February) of 2004/05 and in (b) the summer (June–August) of 2005.

derived from drifter, altimeter, and wind observations is used (Maximenko et al. 2009).

Monthly averaged climatologies are constructed for TMI SST, precipitation, and cloud liquid water and QuikSCAT surface wind velocity for a common period from January 2000 to December 2008. Anomalies are defined as deviations from the climatologies.

## 3. Observational analysis

In the summer of 2004, a large meander first occurred off the south coast of Japan, reached its mature phase in late winter and early spring of 2005, and finally disappeared in the summer of 2005. Figure 1a shows mean SST and SSH in the winter [December–February (DJF)] of 2004/05. A well-developed large meander is found off the south coast of Japan, with a strong cyclonic eddy southeast of Kii Peninsula (centered at 32.5°N, 137°E),

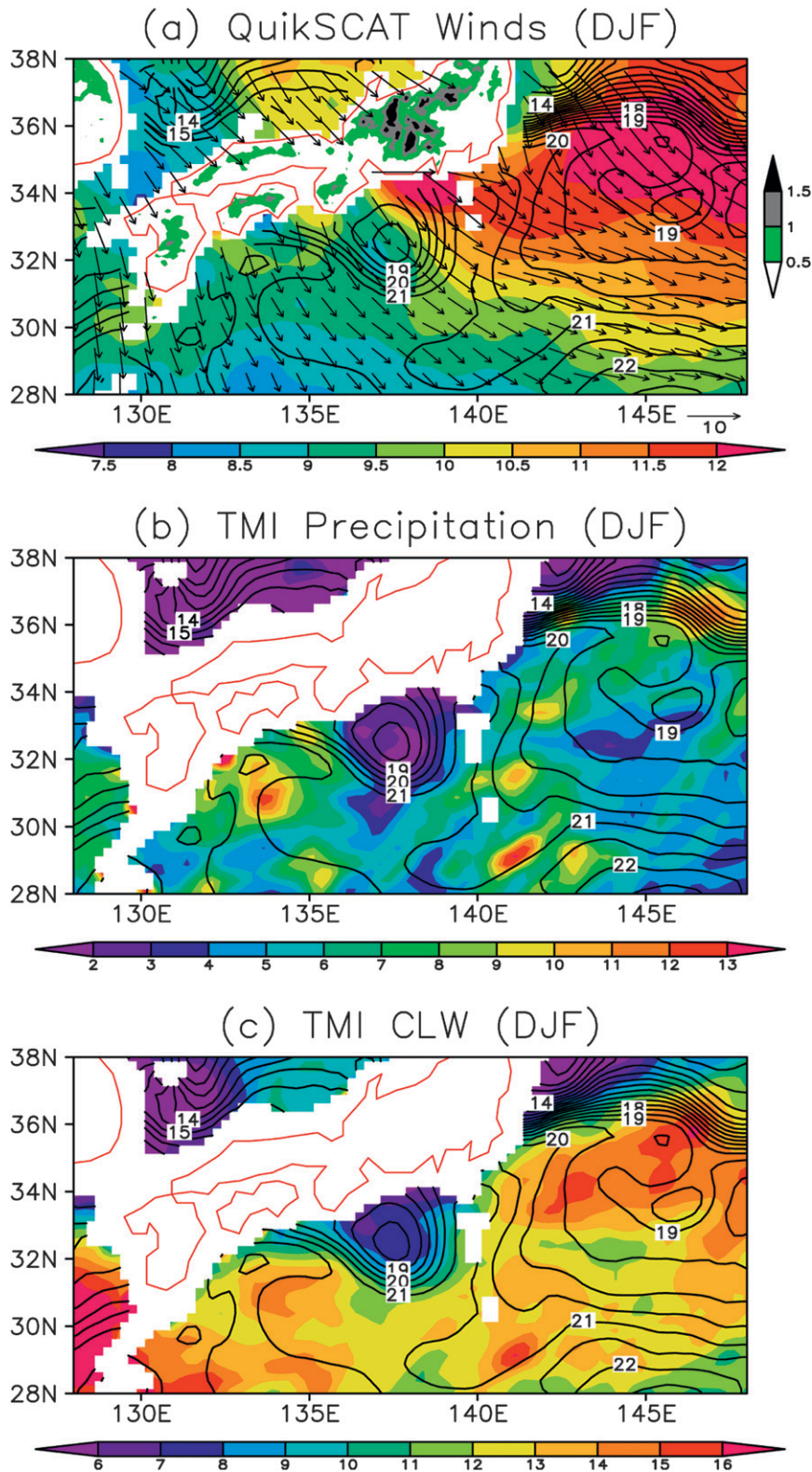


FIG. 2. Seasonal mean (a) QuikSCAT wind velocity ( $\text{m s}^{-1}$ ), (b) TMI precipitation ( $\text{mm day}^{-1}$ ), and (c) TMI column-integrated cloud liquid water ( $10^{-2} \text{ mm}$ ) in DJF of 2004/05. Seasonal mean TMI SSTs are also plotted in contours ( $^{\circ}\text{C}$ ). Topographic heights (shaded, km) are plotted over the land in (a).

and an anticyclonic eddy to its southwest. The meandering Kuroshio leaves a clear signature in winter SST. The SST is  $2^{\circ}\text{--}3^{\circ}\text{C}$  colder over the cyclonic eddy off Kii Peninsula than the surroundings, with a minimum below  $18.5^{\circ}\text{C}$  as opposed to  $21^{\circ}\text{--}22^{\circ}\text{C}$  in the Kuroshio mainstream. The cold SSTs appear due to upwelling, the shoaling thermocline, and a shallow mixed layer in the cyclonic eddy.

Figure 2a shows the QuikSCAT wind field for the winter of 2004/05. Land orography affects coastal winds. Wind speed extremes on the south coast of Japan can generally be matched with upstream mountains. Off the Kii Peninsula, wind speed reaches an offshore minimum over the cool pool left behind by the meandering Kuroshio. As will be shown in section 4, this wind speed reduction is consistent with SST-induced modification of surface pressure gradients and reduction in turbulent mixing. The collocation of wind speed reduction and low SST becomes clear in a map of deviations from the winter climatology (Fig. 3a). This positive SST–wind speed correlation in space can be better seen in the spring of 2005 (not shown). Similar SST-induced wind variations are commonly observed over mesoscale SST features in different regions, such as in the western Arabian Sea (Vecchi et al. 2004), and along oceanic fronts in mid-latitudes, such as the Kuroshio Extension (Nonaka and Xie 2003), Gulf Stream (Chelton et al. 2004), Agulhas Return Current (O’Neill et al. 2003), and Brazil–Malvinas confluence in the South Atlantic (Tokinaga et al. 2005). This positive correlation between SST and wind speed prevails for ocean fronts (Xie 2004; Small et al. 2008), in sharp contrast with the negative correlation often observed on the basin scale in the extratropics that is indicative of atmosphere-to-ocean forcing (Namias and Cayan 1981; Wallace et al. 1990). The positive SST–wind speed correlation indicates the opposite causality: the large meander-induced SST anomalies cause the surface wind to change.

Atmospheric response to SST variations induced by this large meander can also be seen in precipitation (Fig. 2b) and cloud liquid water content (Fig. 2c). Precipitation is in deficit over the cool SST pool off Kii Peninsula. This precipitation “hole” is over 300 km in diameter, with a 70% drop in precipitation ( $2\text{ mm day}^{-1}$  in the hole versus  $7\text{ mm day}^{-1}$  for the background). Similarly, there is a reduction of cloud liquid water content over the cool water between the meandering Kuroshio and Kii Peninsula, with a 50% drop ( $0.06\text{ mm}$  over the cool water versus  $0.12\text{ mm}$  for the background). The effects of the Kuroshio meander on precipitation and cloud are illustrated more clearly in the anomaly maps (Figs. 3b and 3c). Off Kii Peninsula, cold-SST anomalies cause both rainfall and cloud liquid water to decrease. The effect of the SST anomaly on the

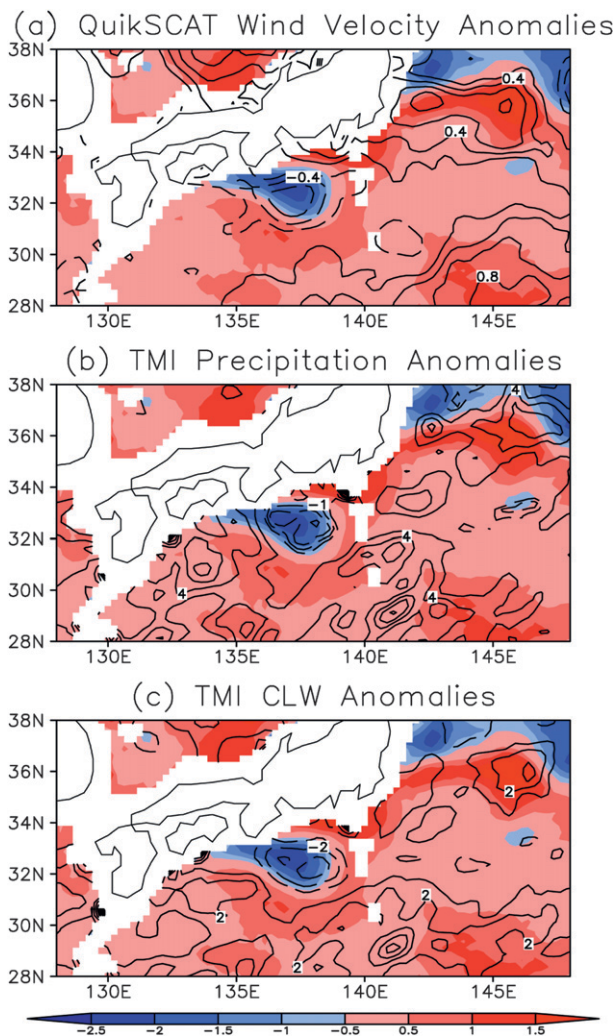


FIG. 3. Seasonal (DJF in 2004/2005) mean anomalies of (a) QuikSCAT wind velocity (contours at  $0.2\text{ m s}^{-1}$  intervals), (b) TMI precipitation [contours at  $2\text{ (}0.5\text{ mm day}^{-1}\text{)}$  intervals for solid (dashed) contours], and (c) TMI column-integrated cloud liquid water content (contours at  $10^{-2}\text{ mm}$  intervals). The DJF mean TMI SST anomalies are also plotted in the shaded region.

cloud liquid water is consistent with the analysis of Norris and Iacobellis (2005) over the North Pacific Ocean and O’Neill et al. (2005) along the Agulhas Return Current.

Figure 4 shows the evolution of the large meander, with its SST and atmospheric effects in the distance–time sections along the line AB in Fig. 1a of altimeter SSH, QuikSCAT wind velocity, and TMI cloud liquid water anomalies together with TMI SST anomalies. Negative SSH anomalies (Fig. 4a) associated with the larger meander first occur in the early summer of 2004, then develop, reach their mature phase around the winter of 2004/05 and early spring of 2005, and finally decay in late summer. The large meander induces SST

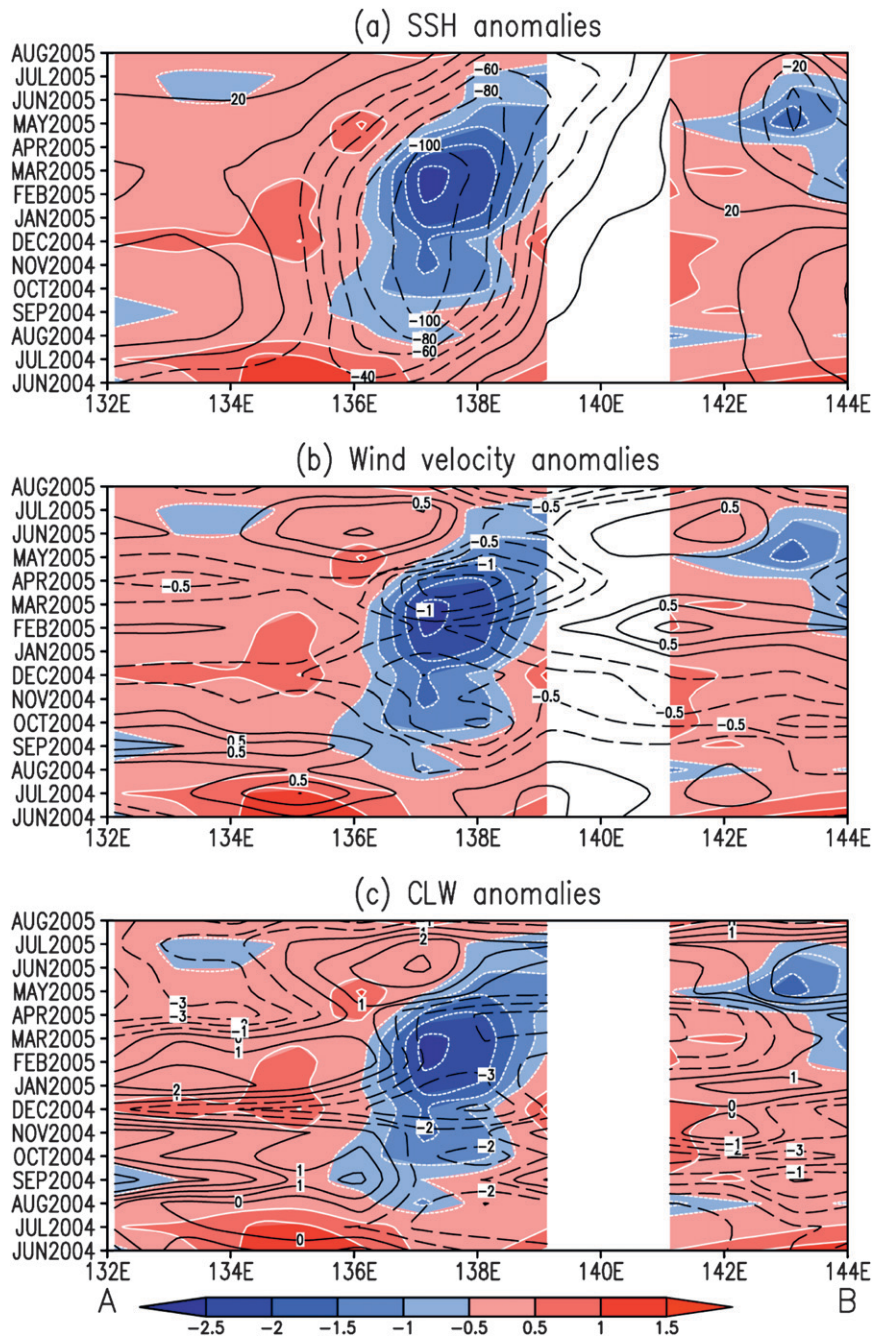


FIG. 4. Time cross sections of (a) SSH (black contours at 20-cm intervals), (b) QuikSCAT velocity (black contours at  $0.25 \text{ m s}^{-1}$  intervals), and (c) TMI cloud liquid water content (black contours at  $10^{-2} \text{ mm}$  intervals) anomalies along the line AB. TMI sea surface temperature anomalies ( $^{\circ}\text{C}$ ) are also plotted in color shading and white contours.

cooling off Kii Peninsula, which in turn decelerates surface winds (Fig. 4b). Negative wind velocity anomalies occur over the negative SST anomalies as early as in summer 2004 when the large meander first appears. These negative wind anomalies are almost in phase with the negative SST anomalies, reaching their peaks

around early spring 2005. However, the LM's effect on cloud and precipitation is mainly limited to its mature phase around the winter of 2004/2005 and early spring of 2005 (Fig. 4c). Even though the larger meander in SSH anomalies is still visible in the summer of 2005, the negative SST anomalies have diminished (Fig. 4a).

The LM's effect on SST displays a clear seasonality with maxima in late winter and early spring. Figure 1b shows SST and SSH in the summer of 2005. In summer, the large meander anomalies in SSH weaken but have a similar pattern to that in winter. The SST anomalies off Kii Peninsula, however, are hardly visible anymore. Thus, the large meander is much longer lasting in dynamical fields (SSH) than in SST. In winter and early spring, the deep ocean mixed layer enhances subsurface ocean dynamical effects on SST by advection and entrainment, while in summer, strong solar radiation shoals the mixed layer, and the reduced dynamical effects allow surface flux to dominate SST variability (Alexander et al. 1999; Tomita et al. 2002; Cassou et al. 2007). The presence or absence of the SST anomaly associated with this large meander explains why the atmospheric effects are strong during winter and early spring and weak during summer.

#### 4. Modeling

##### a. Model and experimental design

We use the Weather Research and Forecasting (WRF) model (version 3.0.1; Skamarock et al. 2005) to examine the large meander's effect on the overlying atmosphere. The model domain is  $19^{\circ}$ – $45^{\circ}$ N,  $119^{\circ}$ – $151^{\circ}$ E. The model uses a horizontal resolution of 15 km and has 39 sigma levels in the vertical. We choose the following set of parameterizations: the Thompson graupel microphysical parameterization (Thompson et al. 2004), the Rapid Radiative Transfer Model (Mlawer et al. 1997), Dudhia schemes for longwave and shortwave radiation calculation (Dudhia 1989), Mellor–Yamada–Janjić (MYJ) turbulence kinetic energy (TKE) scheme (Janjić 1994), and the Kain–Fritsch cumulus parameterization (Kain and Fritsch 1990, 1993). The MYJ surface layer scheme (Janjić 1996, 2002) is used to compute roughness length, friction velocities, exchange coefficients, and sea surface fluxes. This surface layer scheme is based on Monin–Obukhov similarity theory. Surface exchange coefficients for heat, moisture, and momentum are estimated using stability functions from Paulson (1970), Dyer and Hicks (1970), and Webb (1970).

The initial and lateral boundary conditions are obtained from the National Centers for Environmental Prediction (NCEP) Final Analyses (FNL) tropospheric analysis, available on a  $1^{\circ}$  by  $1^{\circ}$  grid with 17 vertical pressure levels. They are interpolated onto the model grid by cubic spline interpolation in the horizontal and linear interpolation in both the vertical and time, based on four times daily analysis. Over the ocean, the Advanced Microwave Scanning Radiometer for Earth Observing System (EOS) (AMSR-E) optimally interpolated daily SSTs on a  $0.25^{\circ}$  by  $0.25^{\circ}$  grid are used as the lower boundary condition.

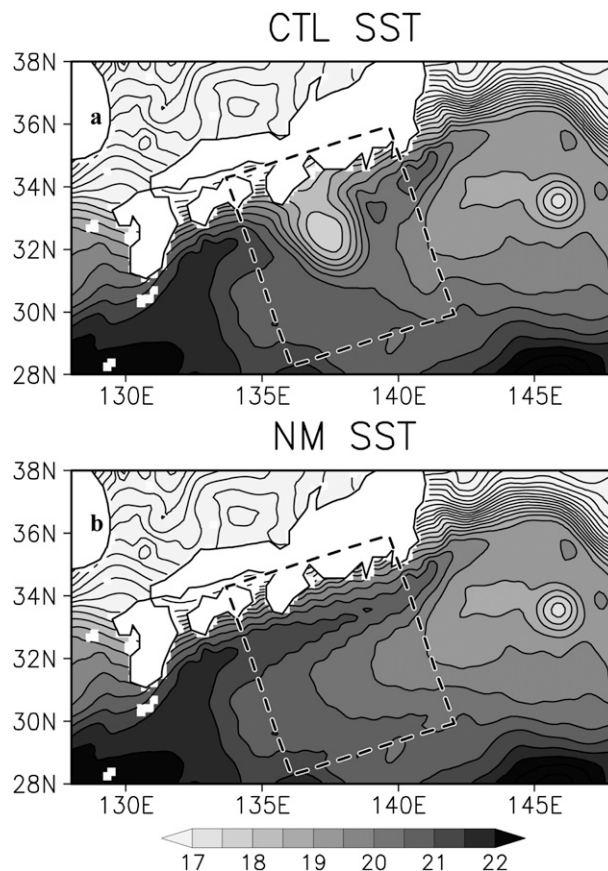


FIG. 5. SST distributions for (a) CTL and (b) NM runs (contours at  $0.5^{\circ}$ C intervals). These SSTs are based on the daily AMSR-E SST and averaged in January 2005.

To examine the effect of the large meander on the overlying atmosphere, we perform two experiments: one with observed SST featuring a SST cooling off Kii Peninsula left behind by the meandering Kuroshio (Fig. 5a) and one with SST modified to remove the SST cooling off Kii Peninsula (Fig. 5b). The SST difference between them is limited to inside the black box in Fig. 5 and vanishes outside. Here, we call the first experiment “control” (CTL) run and the second one a “no meander” (NM) run. Each run is initialized at 0000 UTC 1 January 2005 and integrated through the end of January 2005. We discuss the January means based on 6-hourly output.

##### b. Atmospheric effect of the large meander

The QuikSCAT measures wind stress on the sea surface. The stress is not just related to background wind speed at some height above the surface but also to the static stability (Liu and Tang 1996). However, the stress is related uniquely to the neutral equivalent wind at 10 m. For this reason, the neutral equivalent wind speed

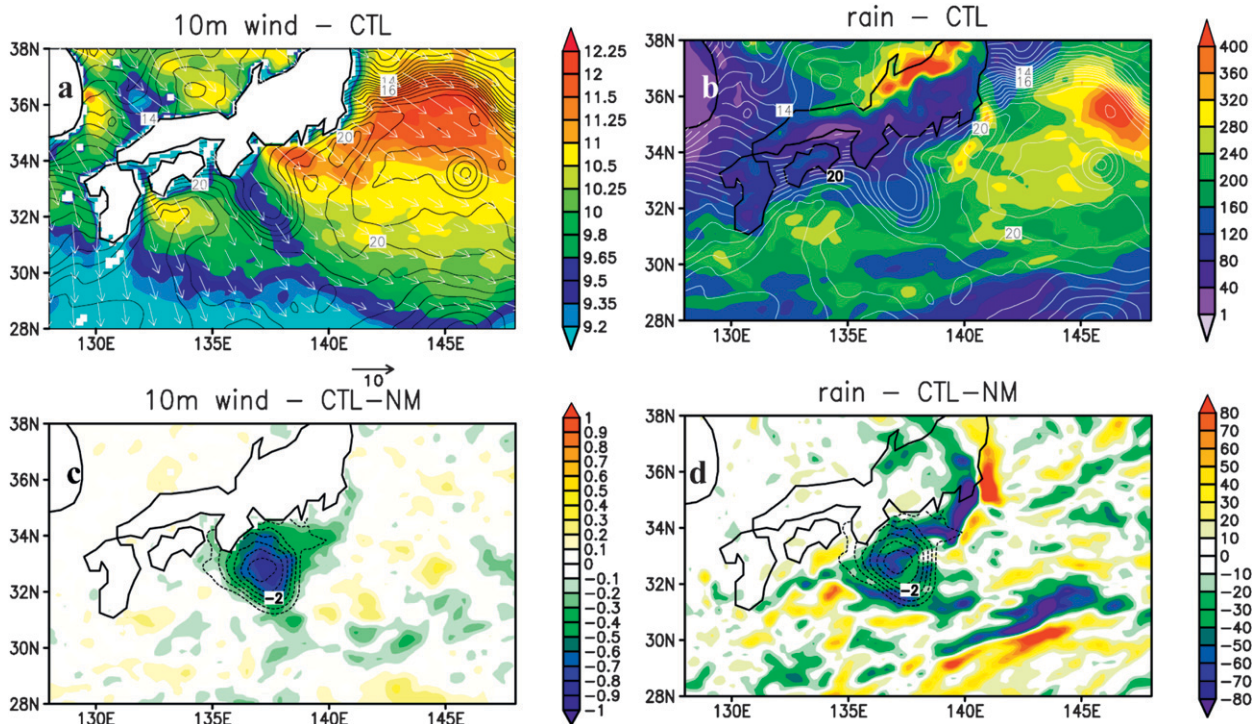


FIG. 6. (a) 10-m neutral equivalent wind velocity (color in  $\text{m s}^{-1}$ ) and wind vectors and (b) precipitation (color in  $\text{mm month}^{-1}$ ) in January 2005, simulated by the model CTL run. (c) 10-m neutral equivalent wind velocity (color,  $\text{m s}^{-1}$ ) and (b) precipitation (color,  $\text{mm month}^{-1}$ ) differences between the CTL and NM runs. Monthly mean SST [solid contours in (a) and (b)] and SST differences [dashed contours in (c) and (d)] between CTL and NM runs are also plotted, respectively.

at 10 m is used to compare the model and observed values of wind velocity near the surface. Figures 6a and 6b present the simulated 10-m surface neutral equivalent wind velocity and precipitation averaged for January 2005. The model simulates well the surface wind field and precipitation off the southeast coast of Japan. In particular, the model captures the reduced wind speeds over the cool SST pool southeast of Kii Peninsula with a minimum of  $9.5 \text{ m s}^{-1}$ , in good agreement with QuikSCAT observations. However, the model slightly underestimates the surface wind speed overall by  $0.5 \text{ m s}^{-1}$ , in comparison with QuikSCAT observations. This deficiency is possibly due to the weak response of vertical turbulent mixing to SST-induced variability in the parameterization of boundary layer turbulence (Song et al. 2009). In addition, the strong underlying surface currents in this region could also contribute to this underestimation by WRF because QuikSCAT measures the actual wind stress on the moving sea surface rather than relative to a stationary sea surface (O'Neill et al. 2005), whereas the sea surface in the WRF model is set to be motionless. The model also captures the reduced precipitation over the cold SST pool. This cold SST effect on surface wind speed and precipitation can be seen more

clearly in the surface wind and precipitation differences between the CTL and NM runs (Figs. 6c and 6d). Negative surface wind speed and precipitation anomalies are collocated with the cold SST anomalies, in good agreement with observations in Fig. 3. These model results clearly indicate the effect of the large meander on the overlying atmosphere.

To further illustrate the effect of the large meander on the overlying atmosphere, the 2-m air temperature, surface sensible, and latent heat fluxes between the CTL and NM runs are shown in Fig. 7. Negative air temperature and sensible and latent heat flux anomalies are found over the cold SST anomalies. The air temperature and sensible and latent flux anomalies follow a similar pattern to that of the SST anomalies. The latent heat flux anomalies reach large magnitudes up to  $140 \text{ W m}^{-2}$  (Fig. 7c), while the sensible heat flux anomalies are as large as  $60 \text{ W m}^{-2}$  (Fig. 7b). The cool-water-induced reduction in precipitation and cloud also increases solar radiation reaching the sea surface (not shown). The reduced surface latent and sensible heat flux, together with increased solar radiation, warm the cool water and, thus, act as negative feedback to LM-induced SST variations. This negative feedback can be clearly seen in the surface

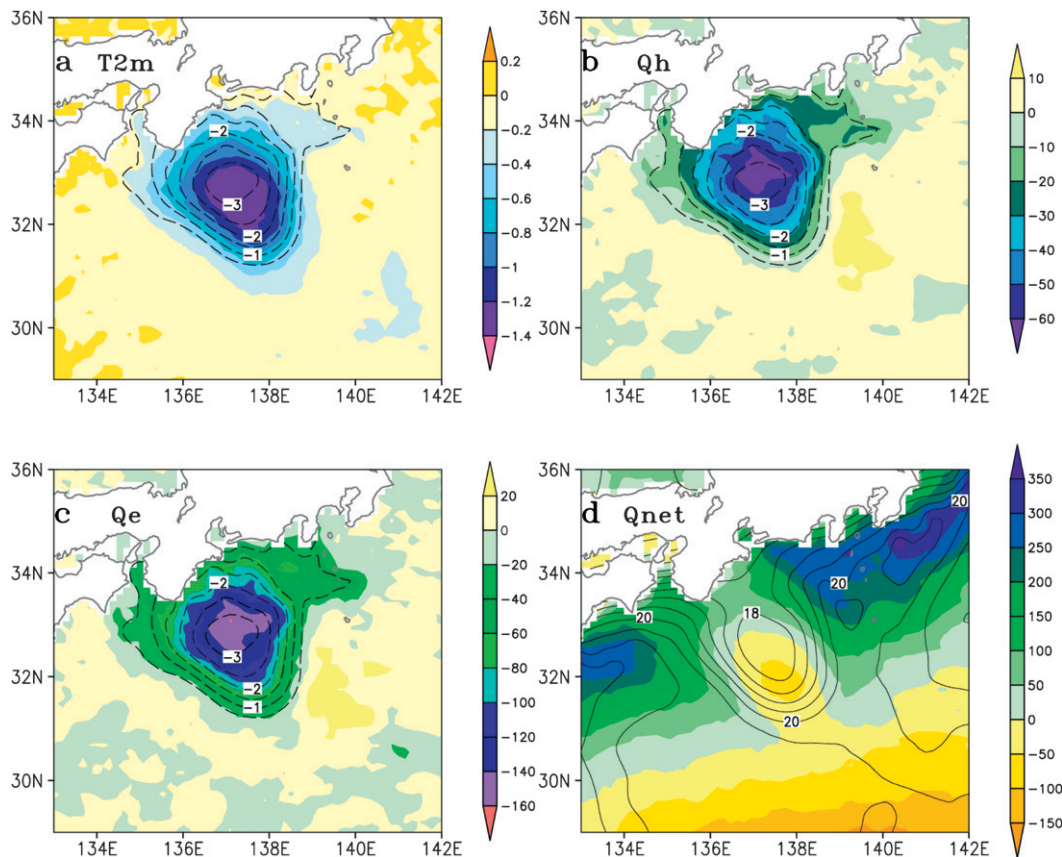


FIG. 7. Monthly mean differences between the CTL and NM runs, superimposed on SST differences in contours ( $^{\circ}\text{C}$ ): (a) 2-m air temperature (shaded,  $^{\circ}\text{C}$ ), (b) surface sensible heat flux (shaded,  $\text{W m}^{-2}$ ), and (c) surface latent heat flux (shaded,  $\text{W m}^{-2}$ ). (d) Monthly mean surface net heat flux (positive upward shaded,  $\text{W m}^{-2}$ ) and SST (contours,  $^{\circ}\text{C}$ ) in the CTL run.

net heat flux in the CTL run (Fig. 7d). While net surface heat flux is strongly upward in winter along much of the Pacific coast of Japan, downward heat flux occurs over the cool pool between Kii Peninsula and the Kuroshio with its maximum magnitude up to  $100 \text{ W m}^{-2}$ . Thus, the atmosphere acts to dampen the cool pool. This supports the notion that ocean hydrodynamics maintains the cool-water pool, which then forces atmospheric variations. The dynamical feedback from the atmospheric variations is not straightforward to evaluate and requires coupled modeling studies, such as the one by Seo et al. (2007) for tropical instability waves.

Located upstream of the prevailing northwesterlies, Japan is not affected much by the Kuroshio meander. During periods of southerly winds, our WRF simulation indicates a cooling on the south coast of central Japan due to enhanced cold advection (not shown). However, the decrease in surface air temperature is less than  $0.5^{\circ}\text{C}$ . The LM's effect on Japanese climate is a subject of our ongoing research.

### c. Surface wind adjustment

There are two possible mechanisms for the atmospheric boundary layer (ABL) to respond to SST anomalies over cool oceans, with SSTs below the convective threshold (say,  $26^{\circ}\text{--}27^{\circ}\text{C}$ ). In the so-called pressure adjustment mechanism (Lindzen and Nigam 1987), SST variations induce wind changes by changing air temperature and forcing pressure gradients in the ABL. In the vertical mixing mechanism of Wallace et al. (1989), on the other hand, a decrease in SST enhances the static stability of the near-surface atmosphere and the reduced vertical turbulent mixing causes increased surface drag, thereby decreasing the near-surface wind speed. In a modeling study of eastern Pacific tropical instability waves, Small et al. (2003) show that, when the thermal advection by prevailing winds is considered, the two mechanisms yield wind anomalies with a similar phase relationship to SST. Some early numerical model simulations were performed to study the atmospheric

response to the Gulf Stream (Wai and Stage 1989; Warner et al. 1990), indicating the importance of the pressure adjustment mechanism. Recent model (Song et al. 2006) and observational (Minobe et al. 2008) studies lend further support for the pressure adjustment mechanism.

Figure 8a presents the differences in sea level pressure (SLP) and surface wind vectors between the CTL and NM runs. Southeast of the Kii Peninsula, cold SST anomalies induce positive SLP anomalies. The SLP maximum is displaced slightly downstream of the SST minimum, an effect due to thermal advection by the prevailing northeasterlies (Small et al. 2003; Fig. 6a). The relatively high SLP over the cold SST pool causes surface wind divergence, which may play a role in suppressing cloud formation and precipitation. A reduction in cloud and precipitation over the cool SST pool is also possibly attributed to a reduction in boundary layer height (not shown), a mechanism first proposed by Wai and Stage (1989). O'Neill et al. (2005) further confirmed that SST-induced cloud formation over the Agulhas Return Current is evidently not due to convection from low-level convergence but from ABL deepening due to increased sensible and latent heat fluxes.

The vector wind response to the SST anomalies shows an anticyclonic tendency and displays clear asymmetry between the northwest and southeast quadrants, dominated by southeasterly and northwesterly anomalies, respectively (Fig. 8a). The following consideration suggests that vector wind anomalies may be understood by combined pressure adjustment and vertical mixing mechanisms. Consider a circular, high pressure center induced by a collocated cold SST pool. In the northeast quadrant, the deceleration of the prevailing northwesterlies induced by reduced vertical mixing reinforces the divergent wind of the high pressure, resulting in strong southwesterly anomalies. In the southwest quadrant, by contrast, the divergence winds induced by vertical mixing and pressure adjustment mechanisms oppose each other; as a result, the northwesterly winds caused by the high pressure dominate. The same argument also explains the asymmetry between the west and east quadrant of the high SLP center, characterized by southeasterly and westerly wind anomalies, respectively. Observed surface wind vector anomalies also exhibit such an asymmetry between the northwest and southeast quadrants of the cold SST pool (Fig. 8b), supporting the resultant effect of pressure adjustment and vertical mixing.

#### d. Momentum budget

We now examine the momentum budget in the surface layer to understand the physical processes for the ABL adjustments to the large meander. The terms of the

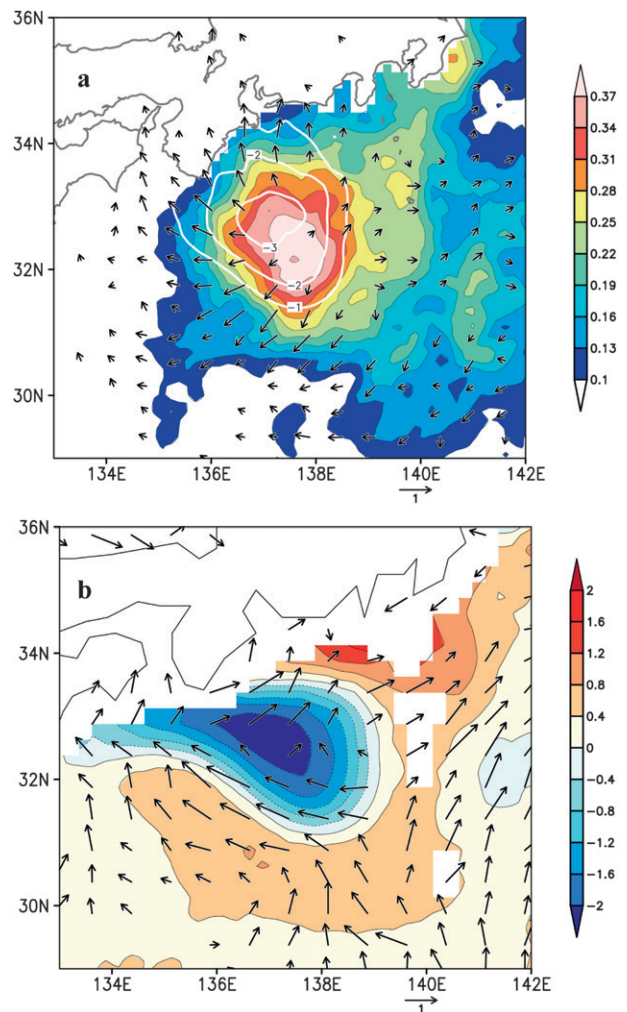


FIG. 8. (a) Monthly mean sea level pressure (color, hPa) and 10-m wind vector ( $\text{m s}^{-1}$ ) differences between the CTL and NM runs in January 2005. Superimposed is the SST difference (white contours of  $-3^\circ$ ,  $-2^\circ$ , and  $-1^\circ\text{C}$ ). (b) November–March anomalies of TMI SST (color,  $^\circ\text{C}$ ) and QuikSCAT surface wind vector.

momentum equation were output every 6 h both in the CTL and NM runs. The horizontal momentum for the mixed layer and free atmosphere can be written as follows:

$$\frac{Du}{Dt} = -\frac{1}{\rho} \frac{\partial p}{\partial x} + fv - \frac{\partial \overline{u'w'}}{\partial z} + D_u$$

and

$$\frac{Dv}{Dt} = -\frac{1}{\rho} \frac{\partial p}{\partial y} - fu - \frac{\partial \overline{v'w'}}{\partial z} + D_v,$$

where  $u$  and  $v$  are the horizontal wind components,  $p$  is pressure,  $\rho$  is air density,  $f$  is the Coriolis parameter,  $u'$  and  $v'$  are turbulent fluctuations of the horizontal wind

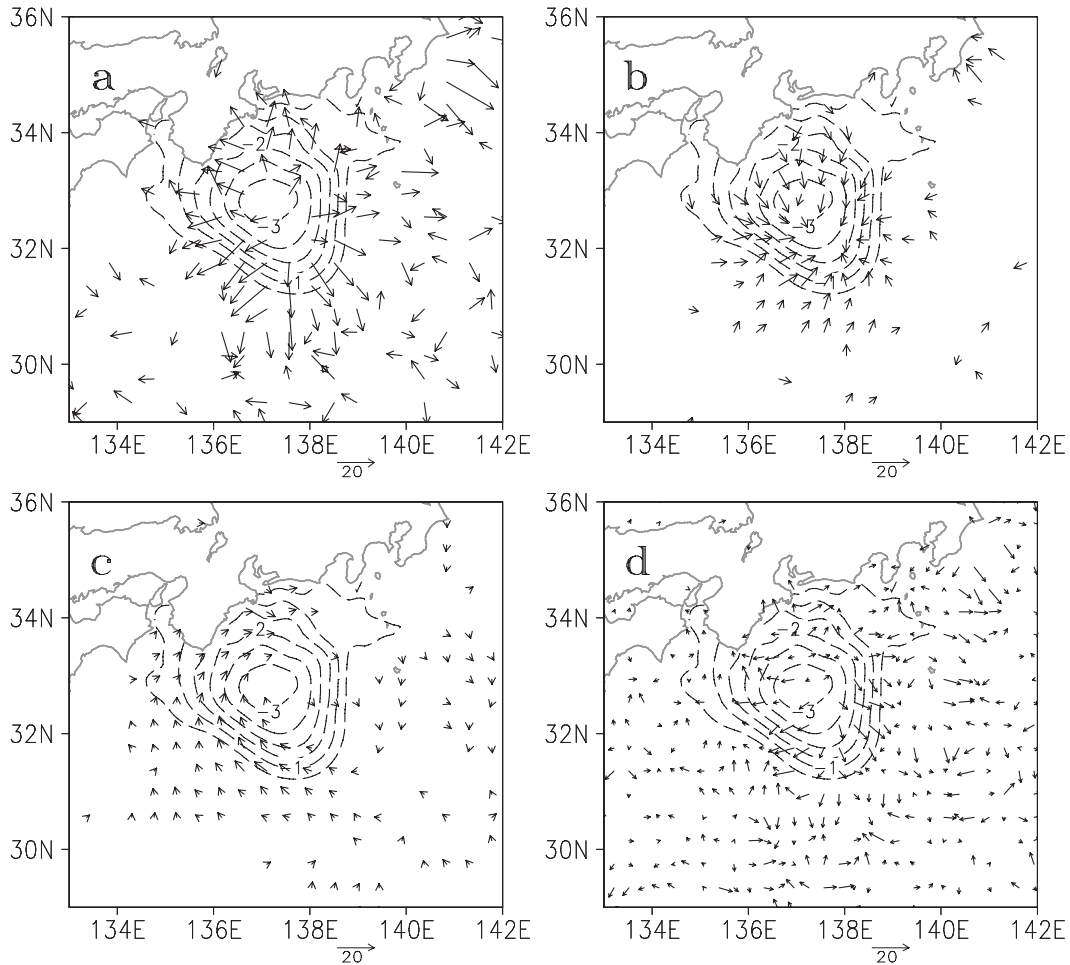


FIG. 9. Dominant terms in the CTL – NM momentum difference budget at the lowest model level (vectors in  $10^{-5} \text{ m s}^{-2}$ ): (a) pressure gradient force, (b) vertical mixing, (c) Coriolis force, and (d) their sum. SST differences between the CTL and NL runs are overlaid as contours ( $^{\circ}\text{C}$ ).

components  $u$  and  $v$ , respectively, and  $w'$  is the fluctuation of the vertical wind. Following the traditional definition, the terms in the above equations represent, from left to right, the acceleration of an air parcel, the pressure gradient force, the Coriolis force, the vertical turbulent momentum flux divergence (referred to as the vertical mixing term), and horizontal mixing. The horizontal mixing terms,  $D_u$  and  $D_v$ , are very small at all levels compared to the other terms. Therefore, only the pressure gradient term, the Coriolis term, and the vertical mixing term are discussed in the following.

Here, we focus on the difference momentum field at the surface. The difference momentum at a given location is defined as the difference momentum at that location for the CTL minus NM. Figure 9 shows the horizontal momentum budget of the difference field as vectors at the lowest model level (about 20 m MSL). The difference momentum is mainly dominated by the perturbation

pressure gradient and the vertical mixing. The pressure gradient (Fig. 9a) shows a divergent pattern with its center slightly shifted downstream from the SST minimum, consistent with the wind response to the positive surface pressure anomalies induced by the cold SST anomalies off the southeast of Kii Peninsula (Fig. 8a). In contrast, the vertical mixing term (Fig. 9b) is directed roughly opposite to that of the pressure gradient and, hence, appears to act as a drag on the pressure-driven flow. As a result, it is the pressure gradient force that acts to reduce the prevailing northwesterly winds over the upwind side of the cold water while accelerating the winds over the downstream side (Fig. 9d), consistent with the pressure adjustment mechanism. Although the Coriolis force is small (Fig. 9c) and does not change the wind speed, it does rotate the difference wind, thus forming an anticyclonic tendency (Fig. 9d). In addition, the sum of these three terms is mainly balanced by horizontal advection.

The downward momentum transport due to SST-induced vertical mixing (Wallace et al. 1989) is difficult to infer from this budget since it is lumped together with the surface drag. Our budget analysis is similar to those of Small et al. (2003) and Koseki and Watanabe (2010). The latter study, by fixing the vertical mixing coefficient in an atmospheric model, reports that SST effects on vertical mixing and SLP are about equally important for surface wind adjustments.

## 5. Conclusions

In the summer of 2004, a large meander event occurred in the Kuroshio path south of Japan for the first time since 1991 and persisted until the next summer. Large meander events are oceanographic in origin and the ocean dynamics has been extensively studied. We have used a suite of satellite observations to document atmospheric effects of this 2004/2005 large meander, thereby extending the literature on Kuroshio path bimodality that has so far been oceanographic only.

The large meander leaves a clear signature in SST except during summer when the mixed layer is shallow and strong surface heating conceals ocean dynamical effects. During the winter of 2004/2005 and early spring of 2005, the SST off Kii Peninsula is more than 2°–3°C cooler than in the core of the Kuroshio, which meanders offshore. Over this cool water pool, surface wind speed, cloud water, and precipitation all decrease. The effect of these atmospheric anomalies is to dampen the cool SST pool.

The WRF model is found to reproduce major features of precipitation and surface wind anomalies observed in January 2005, with reduced surface wind speed and suppressed precipitation over the cold SST pool off Kii Peninsula. Our experiment without the cold SST pool demonstrates that the atmospheric anomalies are, indeed, due to the large-meander-induced SST cooling. Analysis of the perturbation momentum budget shows that near the surface the pressure gradient force and vertical mixing are the dominant terms, with a weaker contribution from the Coriolis force. The pressure gradient force contributes to create the divergent pattern of surface wind, acting to reduce (intensify) the prevailing northwesterly winds over the upwind (downwind) side of the cold SST pool. The vertical mixing is directed roughly opposite to that of the pressure gradient and acts as a drag on the pressure-driven flow. While this vertical mixing effect seems to be dominated by surface friction, the downward momentum transport from aloft would change in response to SST anomaly (Wallace et al. 1989). The quantitative estimate of the vertical momentum transports from aloft and below is a subject of our ongoing research.

*Acknowledgments.* We wish to thank Jan Hafner at IPRC for archiving the TMI and QuikSCAT data from remote sensing systems. We are also grateful to two anonymous reviewers for their constructive comments, which helped improve the paper. This work is supported by a Ministry of Science and Technology 973 Program (2006CB403607), NSFC (40975024), the Japan Agency for Marine-Earth Science and Technology, and NASA.

## REFERENCES

- Akitomo, K., T. Awaji, and N. Imasato, 1991: Kuroshio path variation south of Japan 1: Barotropic inflow–outflow model. *J. Geophys. Res.*, **96**, 2549–2560.
- Alexander, M. A., C. Deser, and M. S. Timlin, 1999: The re-emergence of SST anomalies in the North Pacific Ocean. *J. Climate*, **12**, 2419–2433.
- Cassou, C., C. Deser, and M. A. Alexander, 2007: Investigating the impact of reemerging sea surface temperature anomalies on the winter atmospheric circulation over the North Atlantic. *J. Climate*, **20**, 3510–3526.
- Chao, S.-Y., 1984: Bimodality of the Kuroshio. *J. Phys. Oceanogr.*, **14**, 92–103.
- Chelton, D. B., M. G. Schlax, M. H. Freilich, and R. F. Milliff, 2004: Satellite measurements reveal persistent small-scale features in ocean winds. *Science*, **303**, 978–983.
- Ducet, N., P. Y. Le Traon, and G. Reverdin, 2000: Global high-resolution mapping of ocean circulation from TOPEX/Poseidon and ERS-1 and -2. *J. Geophys. Res.*, **105**, 19 477–19 498.
- Dudhia, J., 1989: Numerical study of convection observed during the winter monsoon experiment using a mesoscale two-dimensional model. *J. Atmos. Sci.*, **46**, 3077–3107.
- Dyer, A. J., and B. B. Hicks, 1970: Flux-gradient relationships in the constant flux layer. *Quart. J. Roy. Meteor. Soc.*, **96**, 715–721.
- Janjić, Z. I., 1994: The step-mountain eta coordinate model: Further developments of the convection, viscous sublayer and turbulence closure schemes. *Mon. Wea. Rev.*, **122**, 927–945.
- , 1996: The surface layer in the NCEP Eta Model. Preprints, *11th Conf. on Numerical Weather Prediction*, Norfolk, VA, Amer. Meteor. Soc., 354–355.
- , 2002: Nonsingular implementation of the Mellor–Yamada level 2.5 scheme in the NCEP Meso model. National Centers for Environmental Prediction Office Note 437, 61 pp.
- Kain, J. S., and J. M. Fritsch, 1990: A one-dimensional entraining/detraining plume model and its application in convection parameterization. *J. Atmos. Sci.*, **47**, 2784–2802.
- , and —, 1993: Convective parameterization for mesoscale models: The Kain–Fritsch scheme. *The Representation of Cumulus Convection in Numerical Models*, K. A. Emanuel and D. J. Raymond, Eds., Amer. Meteor. Soc., 246 pp.
- Kawabe, M., 1985: Sea level variations at the Izu Island and typical stable paths of the Kuroshio. *J. Oceanogr. Soc. Japan*, **41**, 307–326.
- , 1986: Transition processes between the three typical paths of the Kuroshio. *J. Oceanogr. Soc. Japan*, **42**, 174–191.
- , 1996: Model study of flow conditions causing the large meander of the Kuroshio south of Japan. *J. Phys. Oceanogr.*, **26**, 2449–2461.
- Koseki, S., and M. Watanabe, 2010: Atmospheric boundary layer response to the mesoscale SST anomalies in the Kuroshio extension. *J. Climate*, **23**, 2492–2507.

- Lindzen, R. S., and R. S. Nigam, 1987: On the role of sea surface temperature gradients in forcing low level winds and convergence in the tropics. *J. Atmos. Sci.*, **44**, 2418–2436.
- Liu, W. T., and W. Tang, 1996: Equivalent neutral wind. Jet Propulsion Laboratory Publ. 96-17, 16 pp.
- , X. Xie, P. O. Polito, S.-P. Xie, and H. Hashizume, 2000: Atmospheric manifestation of tropical instability waves observed by QuikSCAT and Tropical Rainfall Measuring Mission. *Geophys. Res. Lett.*, **27**, 2545–2548.
- Maximenko, N., P. Niiler, M.-H. Rio, O. Melnichenko, L. Centurioni, D. Chambers, V. Zlotnicki, and B. Galperin, 2009: Mean dynamic topography of the ocean derived from satellite and drifting buoy data using three different techniques. *J. Atmos. Oceanic Technol.*, **26**, 1910–1919.
- Minobe, S., A. Kuwano-Yoshida, N. Komori, S.-P. Xie, and R. J. Small, 2008: Influence of the Gulf Stream on the troposphere. *Nature*, **452**, 206–209.
- Mlawer, E. J., S. J. Taubman, P. D. Brown, M. J. Iacono, and S. A. Clough, 1997: Radiative transfer for inhomogeneous atmosphere: RRTM, a validated correlated-*k* model for the longwave. *J. Geophys. Res.*, **102**, 16 663–16 682.
- Namias, J., and D. R. Cayan, 1981: Large-scale air–sea interactions and short period climate fluctuation. *Science*, **214**, 869–876.
- Nonaka, M., and S.-P. Xie, 2003: Covariations of sea surface temperature and wind over the Kuroshio and its extension: Evidence for ocean-to-atmospheric feedback. *J. Climate*, **16**, 1404–1413.
- Norris, J. R., and S. F. Iacobellis, 2005: North Pacific cloud feedbacks inferred from synoptic-scale dynamic and thermodynamic relationships. *J. Climate*, **18**, 4862–4878.
- O'Neill, L. W., D. B. Chelton, and S. K. Esbensen, 2003: Observations of SST-induced perturbations of the wind stress field over the Southern Ocean on seasonal timescales. *J. Climate*, **16**, 2340–2354.
- , —, —, and F. J. Wentz, 2005: High-resolution satellite measurements of the atmospheric boundary layer response to SST variations along the Agulhas Return Current. *J. Climate*, **18**, 2706–2723.
- Paulson, C. A., 1970: The mathematical representation of wind speed and temperature profiles in the unstable atmospheric surface layer. *J. Appl. Meteor.*, **9**, 857–861.
- Sekine, Y., 1990: A numerical experiment on the path dynamics of the Kuroshio with reference to the formation of the large meander path south of Japan. *Deep-Sea Res.*, **37**, 359–380.
- Seo, H., M. Jochum, R. Murtugudde, A. J. Miller, and J. O. Roads, 2007: Feedback of tropical instability wave-induced atmospheric variability onto the ocean. *J. Climate*, **20**, 5842–5855.
- Skamarock, W. C., J. B. Klemp, J. Dudhia, D. O. Gill, D. M. Barker, W. Wang, and J. G. Powers, 2005: A description of the advanced research WRF version 2. NCAR Tech. Note NCAR/TN-468+STR, 88 pp.
- Small, R. J., S.-P. Xie, and Y. Wang, 2003: Numerical simulation of atmospheric response to Pacific tropical instability waves. *J. Climate*, **16**, 3722–3737.
- , and Coauthors, 2008: Air–sea interaction over ocean fronts and eddies. *Dyn. Atmos. Oceans*, **45**, 274–319.
- Song, Q., P. Cornillon, and T. Hara, 2006: Surface wind response to oceanic fronts. *J. Geophys. Res.*, **111**, C12006, doi:10.1029/2006JC003680.
- , D. B. Chelton, S. K. Esbensen, N. Thum, and L. O'Neill, 2009: Coupling between sea surface temperature and low-level winds in mesoscale numerical models. *J. Climate*, **22**, 146–163.
- Taft, B. A., 1972: Characteristics of the flow of the Kuroshio south of Japan. *Kuroshio—Its Physical Aspects*, H. Stommel and K. Yoshida, Eds., University of Tokyo Press, 165–216.
- Thompson, G., R. M. Rasmussen, and K. Manning, 2004: Explicit forecasts of winter precipitation using an improved bulk microphysics scheme. Part I: Description and sensitivity analysis. *Mon. Wea. Rev.*, **132**, 519–542.
- Tokinaga, H., Y. Tanimoto, and S.-P. Xie, 2005: SST-induced surface wind variations over the Brazil–Malvinas confluence: Satellite and in situ observations. *J. Climate*, **18**, 3470–3482.
- Tomita, T., S.-P. Xie, and M. Nonaka, 2002: Estimates of surface and subsurface forcing for decadal sea surface temperature variability in the mid-latitude North Pacific. *J. Meteor. Soc. Japan*, **80**, 1289–1300.
- Usui, N., H. Tsujino, Y. Fujii, and M. Kamachi, 2008: Generation of a trigger meander for the 2004 Kuroshio large meander. *J. Geophys. Res.*, **113**, C01012, doi:10.1029/2007JC004266.
- Vecchi, G. A., S.-P. Xie, and A. S. Fischer, 2004: Ocean–atmosphere covariability in the western Arabian Sea. *J. Climate*, **17**, 1213–1224.
- Wai, M. M., and S. A. Stage, 1989: Dynamical analyses of marine atmospheric boundary layer structure near the Gulf Stream oceanic front. *Quart. J. Roy. Meteor. Soc.*, **115**, 29–44.
- Wallace, J. M., T. P. Mitchell, and C. Deser, 1989: The influence of sea surface temperature on sea surface wind in the eastern equatorial Pacific: Seasonal and interannual variability. *J. Climate*, **2**, 1492–1499.
- , C. Smith, and Q. Jiang, 1990: Spatial patterns of atmosphere–ocean interaction in the northern winter. *J. Climate*, **3**, 990–998.
- Warner, T. T., M. N. Lakhtakia, J. D. Doyle, and R. A. Pearson, 1990: Marine atmospheric boundary layer circulations forced by Gulf Stream sea surface temperature gradients. *Mon. Wea. Rev.*, **118**, 309–323.
- Webb, E. K., 1970: Profile relationships: The log-linear range, and extension to strong stability. *Quart. J. Roy. Meteor. Soc.*, **96**, 67–90.
- Wentz, F. J., C. Gentemann, D. Smith, and D. Chelton, 2000: Satellite measurements of sea surface temperature through clouds. *Science*, **288**, 847–850.
- Xie, S.-P., 2004: Satellite observations of cool ocean–atmosphere interaction. *Bull. Amer. Meteor. Soc.*, **85**, 195–208.
- Yamagata, T., and S. Umatani, 1989: Geometry-forced coherent structures as a model of the Kuroshio large meander. *J. Phys. Oceanogr.*, **19**, 130–138.